

1 Estimating χ and K_T from fast-response thermistors on traditional shipboard

2 CTDs: sources of uncertainty and bias.

3 Andy Pickering*

4 College of Earth, Ocean, and Atmospheric Sciences, Oregon State University, Corvallis, OR.

5 Jonathan Nash

6 College of Earth, Ocean, and Atmospheric Sciences, Oregon State University, Corvallis, OR.

7 Jim Moum

8 College of Earth, Ocean, and Atmospheric Sciences, Oregon State University, Corvallis, OR.

9 Jen MacKinnon

10 UCSD / Scripps Institute of Oceanography

11 *Corresponding author address: College of Earth, Ocean, and Atmospheric Sciences, Oregon State
University, Corvallis, OR.

13 E-mail:

ABSTRACT

14 The acquisition of turbulence data from traditional shipboard CTD casts is
15 attractive, as it has the potential to dramatically increase the amount of deep-
16 ocean mixing observations globally. While data from shear-probes are eas-
17 ily contaminated by motion of the instrument platform, the measurement of
18 temperature gradient is relatively insensitive to vehicle vibration, making it
19 possible to measure temperature gradient from a shipboard CTD rosette. The
20 purpose of this note is to investigate the error and bias in estimating the rate
21 of dissipation of temperature variance χ and turbulent diffusivity K_T from
22 thermistors mounted on traditional CTD casts. The most significant source
23 of error is associated with the fact that fast-response FP07 thermistors resolve
24 only a fraction of the temperature gradient variance at the fallspeed of typi-
25 cal CTD casts. Assumptions must be made about the wavenumber extent of
26 the temperature gradient spectrum, which scales with the rate of dissipation
27 of turbulent kinetic energy, a quantity that is not directly measured. Here we
28 utilize observations from a microstructure profiler to demonstrate the validity
29 of our method of estimating χ from thermistor data, and to assess uncertainty
30 and bias. We then apply this methodology to temperature gradient profiles
31 obtained from χ pods mounted on a CTD (the CTD- χ -pod), and compare
32 these to microstructure profiles obtained almost synoptically at the equator.
33 CTD- χ -pod estimates of χ compare favorably to the direct microstructure
34 measurements and demonstrate that the χ -pod method is not significantly bi-
35 ased. This supports the utility of the measurement as part of the global repeat
36 hydrography program (GO-SHIP) cruises, during which this type of data has
37 been acquired during the past few years.

³⁸ **1. Introduction**

³⁹ Turbulent mixing affects the distribution of heat, salt, and nutrients throughout the global ocean.

⁴⁰ Diapycnal mixing of cold, dense water with warmer water above maintains the abyssal overturning

⁴¹ circulation (Munk 1966; Munk and Wunsch 1998), which affects global climate. Because the

⁴² turbulence that drives mixing generally occurs at scales that are not resolved in climate models,

⁴³ it must be parameterized, based on either (i) aspects of the resolved model dynamics, (ii) through

⁴⁴ higher resolution models that capture the dynamics that feed energy to turbulence, or (iii) using

⁴⁵ other parameterizations that either dynamically or statistically quantify turbulent fluxes. Recent

⁴⁶ investigations have demonstrated that these models are sensitive to the magnitude and distribution

⁴⁷ of mixing (Melet et al. 2013). A comprehensive set of measurements that spans relevant dynamical

⁴⁸ regimes is needed to constrain mixing and develop more accurate parameterizations.

⁴⁹ Direct measurement of mixing with microstructure profilers equipped with shear probes is ex-

⁵⁰ pensive, time-intensive, and requires considerable care and expertise. Moreover, tethered profilers

⁵¹ can't reach abyssal depths, requiring autonomous instruments to get deeper than \sim 1000-2000 m.

⁵² As a result, existing measurements of diapycnal mixing, especially in the deep ocean, are sparse

⁵³ (Waterhouse et al. 2014). In order to obtain a larger quantity of mixing estimates, considerable

⁵⁴ work has gone into inferring mixing from measurements of the outer scales of turbulence, which

⁵⁵ are easier to obtain. One ~~popular~~ method is the use of Thorpe scales, where diapycnal mixing is

⁵⁶ inferred from inversions in profiles of temperature or density (Thorpe 1977; Dillon 1982). The

⁵⁷ size of resolvable overturn is limited by the profiling speed and instrument noise (Galbraith and

⁵⁸ Kelley 1996). Several studies indicate relatively good agreement with microstructure and other

⁵⁹ observations, ~~but there are some~~ questions about the validity of the method and the assumptions

⁶⁰ made (Mater et al. 2015; Scotti 2015). Parameterizations based on profiles of shear and/or strain

have also been developed and applied to estimate diapycnal mixing (Gregg 1989; Kunze et al. 2006; Polzin et al. 2013; Whalen et al. 2012, 2015). However, they rely on a series of assumptions about the cascade of energy from large to small scales that are often violated; numerous studies (i.e., Waterman et al. (2013)) have shown that there is significant uncertainty associated with these parameterizations, in that there can be a consistent bias in a particular region, yet the sense of the bias (i.e., overpredict vs. underpredict) is not known a priori.

Quanitifying turbulence from velocity shear variance (to compute the dissipation rate of turbulent kinetic energy ε) is challenging on moorings or profiling platforms because there is usually too much vibration and/or package motion for shear-probes to be useful. Other methods (i.e., optics or acoustics) may hold some promise, but lack of scatterers often precludes this type of measurement, especially in the abyss. In addition, shear probes only provide ε , not the mixing of scalars, K , which is often inferred from ε by assuming a mixing efficiency Γ (Osborn 1980) as $K = \Gamma \varepsilon / N^2$, which N^2 is the buoyancy frequency. A more direct measure of turbulent mixing is obtained from the dissipation rate of temperature variance χ (Osborn and Cox 1972). This has the advantage that (i) the temperature and temperature gradient can be computed and are relatively straightforward to measure, and (ii) the estimation of mixing from χ does not require assumptions about Γ . However, the spectrum of temperature gradient extends to very small scales, so that its spectrum is seldom fully resolved (and unlike shear variance, the wavenumber extent of the temperature gradient spectrum does not scale with its amplitude, but instead depends on ε). Assumptions about the spectral shape (Kraichnan vs. Batchelor, and the value of the “constant” q) and its wavenumber extent (governed by the Batchelor wavenumber $k_b = [\varepsilon / (v D_T^2)]^{1/4}$ (Batchelor 1959)) are thus necessary to determine χ unless measurements capture the full viscous-diffusive subrange of turbulence (i.e., down to scales $\Delta x \sim 1/k_b \sim 1\text{mm}$), a criterion seldom achieved. To resolve this, we follow Al-

⁸⁴ ford and Pinkel (2000) and Moum and Nash (2009) and make the assumption that $K_T = K_\rho$ to
⁸⁵ determine the dissipation rate as $\varepsilon_\chi = (N^2\chi)/(2\Gamma < dT/dz >^2)$, permitting k_b to be estimated.

⁸⁶ The goal of this paper is to outline and validate the methods used to compute χ and K_T with
⁸⁷ χ -pods mounted on CTDs. We do this by applying our processing methodology to profiles of tem-
⁸⁸ perature gradient measured by thermistors on the ‘Chameleon’ microstructure profiler, which pro-
⁸⁹ vides a direct test of our methodology. Because Chameleon is a loosely tethered profiler equipped
⁹⁰ with shear probes (Moum et al 1995), it directly measures ε and allows us to test our assumptions.
⁹¹ Specifically, it allows us to determine biases associated with computing χ from partially-resolved
⁹² temperature alone, as compared to ~~that when it is computed by including knowledge of the dissi-~~
⁹³ ~~pation rate,~~ which constrains the wavenumber extent of the scalar spectra. After establishing that
⁹⁴ the method works, we then compare CTD- χ pod profiles to nearby microstructure profiles.

⁹⁵ 2. Data

⁹⁶ a. EQ14

⁹⁷ Data were collected on the R/V Oceanus in Fall 2014 during the EQ14 experiment to study
⁹⁸ equatorial mixing. More than 2700 Chameleon profiles were made, along with 35 CTD- χ pod
⁹⁹ profiles bracketed by Chameleon profiles in order to maintain calibrations during the cruise. Most
¹⁰⁰ Chameleon profiles were made to a maximum depth of about 250m, with CTD casts going to
¹⁰¹ 500m or deeper. The EQ14 experiment and results are discussed in more detail in (SJ Warner, RN
¹⁰² Holmes, EH McHugh-Hawkins, JN Moum, 2016: Buoyant gravity currents released from tropical
¹⁰³ instability waves, JPO, in preparation).

104 **3. Methods**

105 As mentioned in the introduction, the temperature gradient spectrum is rarely fully resolved
106 down to the small scales of turbulent mixing. The fraction of the spectrum resolved depends on
107 the true spectrum (a function of χ and ε), the flowspeed past the sensor (u), and the response of
108 the thermistor. The GE/Thermometrics FP07 thermistors we use typically resolve frequencies up
109 to about $f_{max} = 10 - 15$ Hz. The maximum resolved wavenumber is then equal to $k_{max} = f_{max}/u$,
110 while the wavenumber extent of the true spectrum varies with k_b (and $\varepsilon^{1/4}$). At the typical vertical
111 fall rate of a CTD rosette (~ 1 m/s), only about 20% of k_b is resolved at $\varepsilon = 10^{-10} W kg^{-1}$ (Figure)

112 2). While methods have been developed to fit the observed temperature gradient spectrum to
113 theoretical forms (Ruddick et al. 2000), these work only when a larger fraction of the temperature
114 gradient spectrum is resolved. For the relatively high profiling speeds typical of CTD casts, we
115 find these methods do not work well (see appendix for details) and therefore we use the following
116 methodology, which does not have a strongly ε -dependent bias.

117 We first outline our method for estimating χ , which relies on (i) determining the instantaneous
118 flowspeed past the sensor, (ii) identifying periods where the signals may be contaminated by the
119 wake of the CTD rosette, (iii) defining the relevant N^2 and $(dT/dz)^2$, and (iv) applying an iterative
120 method to compute χ and K_T . We then discuss some limitations and practical considerations that
121 arise.

122 *a. Iterative Method for estimating χ*

123 For each ~ 1 second window, χ is estimated via the following procedure as outlined in Moum
124 and Nash (2009). For isotropic turbulence,

$$\chi_T = 6D_T \int_0^\infty \Psi_{T_x}(k) dk \quad (1)$$

125 where D_T is the thermal diffusivity and $\Psi_{T_x}(k)$ is the wavenumber spectrum of dT/dx .

126 Note that dT/dx is not actually measured; dT/dt is measured, and dT/dx is inferred from

127 Taylor's frozen flow hypothesis:

$$\frac{dT}{dx} = \frac{1}{u} \frac{dT}{dt} \quad (2)$$

128 The wavenumber extent of the spectrum depends on the Batchelor wavenumber k_b , which is
129 related to ε :

$$k_b = [\varepsilon / (v D_T^2)]^{1/4} \quad (3)$$

130 We assume that $K_\rho = K_T$ and $K_\rho = \Gamma \varepsilon / N^2$. Then dissipation rate is computed as

$$\varepsilon_\chi = \frac{N^2 \chi_T}{2\Gamma \langle dT/dz \rangle^2} \quad (4)$$

131 Typical thermistors do not resolve the spectrum out to k_b , so the measured spectrum is fit to the
132 Kraichnan form of theoretical scalar spectrum over the range of resolved wavenumbers ($k_{min} <$
133 $k < k_{max}$). The variance between the measured $[\Phi_{T_x}(k)]_{obs}$ and theoretical $[\Phi_{T_x}(k)]_{theory}$ spectra at
134 these wavenumbers is assumed to be equal:

$$\int_{k_{min}}^{k_{max}} [\Phi_{T_x}(k)]_{obs} dk = \int_{k_{min}}^{k_{max}} [\Phi_{T_x}(k)]_{theory} dk \quad (5)$$

135 An iterative procedure is then used to fit and calculate χ and ε :

136 1. First we estimate χ_T based on an initial guess of $\varepsilon = 10^{-7}$ Wkg⁻¹ and compute k_b via eq. 3.

137 We set $k_{max} = k_b/2$ or to a wavenumber equivalent to $f_{max} = 7$ Hz [i.e., $k_{max} = 2\pi(f_{max})/u$],
138 whichever is smaller. In general f_{max} should be the highest value which is safely below the
139 sensor's roll-off. We chose $f_{max} = 7$ Hz in this case based on inspection of the temperature
140 gradient spectra and historical measurements of these sensors (see appendix for more details).

141 2. We then use Eq. (4) to refine our estimate of ε and k_b and recompute χ_T using Eqs. (1) and
142 (5).

143 3. This sequence is repeated and converges after two or three iterations.

144 Note that this procedure is equivalent to the explicit formulation of (Alford and Pinkel 2000),
145 except we use the Kraichnan theoretical form instead of the Batchelor spectrum for $[\Phi_{T_x}(k)]_{theory}$.

146 **b. CTD- χ pod Data Processing**

147 The basic outline for processing each CTD- χ -pod profile is as follows:

148 1. The correct time-offset for the χ -pod clock is determined by aligning highpass-filtered dp/dt
149 from the 24Hz CTD data to integrated vertical accelerations measured by the χ -pod. χ -pod
150 clock drift is small, typically on the order of 1 sec/week, but it is imperative to get records
151 aligned within < 0.5 s so that the correct $u = w = \cancel{dp/dt}$ is used.

152 2. Low-order polynomial calibration coefficients are determined to convert thermistor voltages
153 from χ pod to ITS90 temperature (as measured by the CTD). Figure 4 shows an example of
154 the aligned and calibrated CTD- χ pod timeseries for one cast. Note the significant differences
155 in amount of variance associated with the two sensors during down and up casts. For the
156 upward-mounted sensor (T1), the downcast signal is largely associated with the CTD wake,
157 as is the upcast for the downward-mounted sensor (T2). Only the ‘clean’ portions of the cast
158 (e.g., the T1 upcast and the T2 downcast) are used in the χ pod calculations.

159 3. Depth loops are identified and flagged in the 24Hz CTD data Figure 3. χ -pod data during
160 these times are discarded since the signals are likely contaminated by the wake of the CTD.
161 We use a vertical velocity threshold of 0.3m/s and throw out data within 2m of the identified
162 loops. Even for profiles that are significantly affected by ship heaving, good segments of data
163 are obtained over a majority of the depths after removing contaminated data, allowing us to
164 compute values in nearly every 10m bin.

165 4. Buoyancy frequency N^2 and temperature gradient dT/dz are computed from 1-m binned
166 CTD data, and averaged over a scale of 10m. The results are not very sensitive to the averag-
167 ing interval (see appendix for more details).

168 5. Half-overlapping 1 sec windows of data are used to estimate χ and K_T following the methods
169 described in Moum and Nash (2009), as outlined in the previous section.

170 *c. Example Spectra and Fits*

171 Examples of the observed and fit spectra are shown in Figure 5, for low and high dissipation
172 rate. Note that at lower ε , a larger fraction of k_b is observed and the peak of the spectrum is ~~nearly~~
173 resolved. At higher ε , less of the spectrum is resolved and the spectral peak is well above the
174 maximum resolved wavenumber. Even so, the iterative χ pod method gives an accurate estimate
175 of χ . The χ pod and Chameleon fits are performed over the same wavenumber range and match
176 there. However, the higher-wavenumber portions of the fit spectra differ since the Chameleon fits
177 use the observed k_b to determine the wavenumber extent.

178 *d. flowspeed past the sensor*

179 The flowspeed past the thermistor is needed to convert the measured temperature derivative
180 dT/dt to a spatial gradient. For the CTD- χ pod, the largest contribution to the flowspeed is usu-
181 ally the vertical velocity of the CTD package (dp/dt), which is close to 1m/s on average, so we
182 typically neglect the horizontal component of velocity in converting from frequency to wavenum-
183 ber spectra. Although usually a good approximation, errors may be introduced where horizontal
184 velocities are large. Note that because it is the total instantaneous velocity magnitude that repre-
185 sents flow past the sensor, neglecting the horizontal component of velocity (assuming $u = dp/dt$)
186 means we ~~are~~ always underestimating the true flowspeed past the sensor. When the CTD package

is equipped with LADCP, the true flowspeed can be measured. In some cases (including EQ14) where the CTD was not equipped with LADCP, it would seem that the ship's ADCP could be used to estimate the horizontal component of velocity. However, because the CTD does not travel perfectly vertically in strong currents, this is difficult to do in practice. In a strong horizontal flow, the CTD will drift with the current while descending, lowering the flow relative to the sensors. On the upcasts, the CTD will be pulled against the current, increasing the flow relative to the sensors. Since the CTD in EQ14 was not equipped with LADCP, we use dp/dt as the flowspeed, and estimate potential errors in the appendix.

4. Results

a. Direct Test of χ pod Method

We begin by utilizing the highly-resolved ~~turbulence profiler~~ data (for which both ε and χ are measured) to test the assumptions in our method of estimating χ . We first apply the χ pod method to each Chameleon profile, using only the FP07 thermistor data. These results, which we ~~will~~ refer to as χ_{χ} , are then compared with χ_{ε} , computed by integrating the theoretical temperature gradient spectrum with k_b computed directly from shear-probe derived ε . Qualitatively, χ_{χ} and χ_{ε} show very similar depth and time patterns (Figure 6) and appear to agree in magnitude, ~~suggesting the method works well~~. A more quantitative comparison is made with a 2-D histogram (Figure 7), showing the two are well-correlated over a wide range of magnitudes. The distribution of \log_{10} of the χ ratios is approximately normal, with a mean of $\mu = -0.1$ and standard deviation of $\sigma = 0.51$.

b. CTD χ -pod - Chameleon Comparison

Having demonstrated that the method works using Chameleon data, we now compare χ from CTD-mounted χ pods to χ_{ε} . In contrast to the Chameleon data, the CTD is more strongly coupled

209 to the ship, and therefore subject to more vibration, heaving, and artificial turbulence created by the
210 rosette. A total of 35 CTD- χ pod casts were performed, bracketed with Chameleon profiles imme-
211 diately before and after. We first compare CTD- χ pod profiles to the mean of the two Chameleon
212 profiles bracketing each cast, both averaged in 5m depth bins (Figure 8). The two are correlated,
213 with considerable scatter. A histogram of the log of ratios is approximately normal and has a mean
214 of -0.31 , indicating a possible small negative bias. Since we expect significant natural variability
215 even between adjacent Chameleon profiles, we investigate further to determine if the observed
216 χ pod variability is of a similar magnitude or greater than expected. Scatter plots of before vs.
217 after Chameleon profiles (not shown), typically separated by about an hour, show a similar level
218 of scatter as the differences between methods, suggesting that the observed differences (Figure
219 8) can be explained by natural variability in turbulence. This is demonstrated by histograms of
220 the ratio of χ from adjacent casts (Figure 9) which show that the variability between CTD χ pod
221 and Chameleon casts is similar to the natural variability between before/after Chameleon profiles.
222 Profiles from all CTD-Chameleon pairs averaged in time and 40m depth bins (Figure 10) overlap
223 within 95% confidence limits at all depths where there exists good data for both. Averages of sub-
224 sets of these profiles that were clustered in position/time (not shown) also agree well. We conclude
225 that the variability between CTD χ pod and Chameleon profiles is indistinguishable from natural
226 variability in turbulence levels.

227 5. Discussion

228 We have shown that χ can be accurately estimated from χ pods attached to CTD rosettes. The
229 method also estimates ε , but we have not discussed it here since it involves more assumptions
230 and uncertainties. One major assumption is the mixing efficiency Γ . A value of 0.2 is commonly
231 assumed, but evidence suggests this may vary significantly. Moum and Nash (2009) found a bias

232 of up to 1.6 for Γ values ranging from 0.1 to 0.35. Another major assumption in the χ pod method
233 is that $K_T = K_\rho$. Preliminary investigation on this data suggests that this assumption does not
234 hold here and may be responsible for a negative bias in ϵ , but more work is needed to verify this.
235 However we have shown that even if ϵ estimates are biased, χ and K_T are still robust.

236 The goal of CTD- χ pods is to expand the number and spatial coverage of ocean mixing obser-
237 vations. We have already deployed instruments during several process experiments and on several
238 GO-SHIP repeat-hydrography cruises. We plan to continue regular deployment on GO-SHIP and
239 similar cruises, adding χ and K_T to the suite of variables regularly measured. The expanding
240 database of mixing measurements from CTD- χ pods will also enable testing of other commonly-
241 used or new mixing parameterizations. This has the potential to be transformative for the field,
242 allowing the community to develop and test global turbulence parameterizations, use estimates of
243 turbulence along with the CLIVAR repeat hydrography data for inverse models and water mass
244 modification calculations, identify hotspots of turbulence to target with future process experi-
245 ments, and compare with in-situ chemical and biological measurements made routinely on repeat
246 hydrography cruises.

247 6. Conclusions

- 248 • The χ pod method for estimating χ and K_T was directly applied to temperature gradients
249 measured by the Chameleon microstructure profiler on > 2700 profiles during the EQ14
250 cruise. The estimated χ_χ agrees well with χ_ϵ calculated using ϵ from shear probes over a
251 wide range of magnitudes (Figure 7) with little or no bias, demonstrating that the method
252 works.
- 253 • CTD- χ pod profiles were also compared to nearby Chameleon profiles during the cruise. Vari-
254 ability between CTD- χ pod and Chameleon estimates of χ is indistinguishable from natural

variability between Chameleon profiles. Time-averaged profiles of χ from both platforms agree within 95% confidence limits, and no significant bias was detected between the estimates of χ .

- We conclude that estimates of χ and K_T made from the CTD- χ pod platform are robust and reliable.

Acknowledgments. The EQ14 experiment was funded by [???](#). We thank the Captain and crew of R/V Oceanus. Also thank people [who helped collect the data, those who made the sensors, etc..](#)

APPENDIX A

Sensitivity Analysis

A1. Flowspeed Past Sensor

To quantify the potential error in the χ pod calculations from ignoring horizontal velocities and assuming the flow speed is equal to the vertical speed of the CTD rosette, we repeated the calculations with constant offsets added to the flowspeed. Since the total magnitude of velocity is used, dp/dt is a minimum estimate of the true speed. Adding 0.1(1)m/s results in a mean percent error of 14(58) percent (Figure 11), small compared the large natural variability in turbulence and uncertainty in our measurements. Note that increasing the velocity tends to result in smaller values of χ , since it shifts the spectrum to lower wavenumbers.

We also looked for any systematic biases associated with flowseed. We found the χ was biased high for very small speeds ($u < 25\text{cm/s}$). This could be associated with contamination by CTD wake or entrained water when the CTD slows. These values were discarded for our analysis.

275 **A2. N^2 and dT/dz**

276 We investigated the sensitivity of the calculations to the scale over which N^2 , dT/dz are aver-
277 aged. The iterative method to estimate chi requires the background stratification N^2 and tempera-
278 ture gradient dT/dz . The estimate of χ is insensitive to these scales. However, while dissipation
279 rate ε and diffusivity K_T are more strongly affected because they are linearly related to these val-
280 ues. Computing N^2 and dT/dz over smaller scales (less than a few m) results in larger values and
281 hence some larger values of K_T .

282 **APPENDIX B**

283 **Test of MLE fitting method**

284 We also tested the spectrum fitting method of Ruddick et al. (2000) and compared to our χ_{pod}
285 method. The MLE method works well and gives similar results to our method at true ε values
286 less than about 10^{-9} , but severely underestimates χ at larger values of epsilon, where only a small
287 fraction of the spectrum is resolved (Figure 12). At lower profiling speeds we would expect the
288 MLE method to work better, as more of the spectrum will be resolved for a given value of epsilon.

289 **APPENDIX D**

290 **Thermistor Frequency Response**

291 Prior to 2009, the transfer function for each FP07 thermistor was measured by profiling adjacent
292 to a thermocouple in Yaquina Bay, OR. However, measuring the transfer function for each indi-
293 vidual thermistor proved too expensive and time-consuming, and since that time a generic transfer
294 function has been used. Figure 13 shows the measured transfer functions for 2008. The majority
295 of the ~~the~~ transfer functions are similar for ~~at~~ frequencies up to about 10 Hz, and begin to sig-

nificantly differ above that. To estimate the potential error in not using a transfer function, we
calculated the % of spectral variance captured for each of the measured functions. For frequencies
up to 7Hz, more than 95% is captured for 88% of the measured functions. If frequencies up to
15hz are used, more than 95 % variance is captured only 67% of the time. Using only frequencies
up to 7Hz (where the transfer function is equal to or very close to unity) avoids the issue of the
unknown transfer functions.

References

- Alford, M., and R. Pinkel, 2000: Patterns of turbulent and double diffusive phenomena: Observations from a rapid profiling conductivity probe. *J. Phys. Oceanogr.*, **30**, 833–854.
- Batchelor, G. K., 1959: Small-scale variation of convected quantitites like temperature in turbulent fluid. *J. Fluid Mech.*, **5**, 113–139.
- Dillon, T. M., 1982: Vertical overturns: A comparison of Thorpe and Ozmidov length scales. *J. Geophys. Res.*, **87**, 9601–9613.
- Galbraith, P. S., and D. E. Kelley, 1996: Identifying overturns in CTD profiles. *J. Atmos. Ocean. Tech.*, **13**, 688–702.
- Gregg, M., 1989: Scaling turbulent dissipation in the thermocline. *J. Geophys. Res.*, **94 (C7)**, 9686–9698.
- Kunze, E., E. Firing, J. Hummon, T. K. Chereskin, and A. Thurnherr, 2006: Global abyssal mixing inferred from lowered ADCP shear and CTD strain profiles. *Journal of Physical Oceanography*, **36 (8)**, 1553–1576.

- 316 Mater, B. D., S. K. Venayagamoorthy, L. S. Laurent, and J. N. Moum, 2015: Biases in Thorpe scale
317 estimates of turbulence dissipation Part I: Assessments from large-scale overturns in oceanographic
318 data. *J. Phys. Oceanogr.*, **45** (2015), 2497–2521.
- 319 Melet, A., R. Hallberg, S. Legg, and K. L. Polzin, 2013: Sensitivity of the ocean state to the
320 vertical distribution of internal-tide-driven mixing. *J. Phys. Oceanogr.*, **43** (3), 602–615, doi:
321 <http://dx.doi.org/10.1175/JPO-D-12-055.1>.
- 322 Moum, J., and J. Nash, 2009: Mixing measurements on an equatorial ocean mooring. *J. Atmos.*
323 *Ocean. Tech.*, **26**, 317–336.
- 324 Munk, W., and C. Wunsch, 1998: Abyssal recipes II: energetics of tidal and wind mixing. *Deep-*
325 *Sea Res. Part I*, **45**, 1977–2010.
- 326 Munk, W. H., 1966: Abyssal recipes. *Deep-Sea Res.*, **13**, 707–730.
- 327 Osborn, T. R., 1980: Estimates of the local rate of vertical diffusion from dissipation measure-
328 ments. *J. Phys. Oceanogr.*, **10**, 83–89.
- 329 Osborn, T. R., and C. S. Cox, 1972: Oceanic fine structure. *Geophys. Fluid Dyn.*, **3**, 321–345.
- 330 Polzin, K. L., A. C. Naveira Garabato, T. N. Huussen, B. M. Sloyan, and S. N. Waterman, 2013:
331 Finescale parameterizations of turbulent dissipation. *Rev. Geophys.*, **submitted**.
- 332 Ruddick, B., A. Anis, and K. Thompson, 2000: Maximum likelihood spectral fitting: The Batch-
333 elor spectrum. *J. Atmos. Ocean. Tech.*, **17**, 1541–1555.
- 334 Scotti, A., 2015: Biases in Thorpe scale estimates of turbulence dissipation Part II: Energetics
335 arguments and turbulence simulations. *J. Phys. Oceanogr.*, **45** (2015), 2522–2543.

- 336 Thorpe, S., 1977: Turbulence and mixing in a Scottish Loch. *Philos. Trans. R. Soc. London Ser.*
337 *A*, **286**, 125–181.
- 338 Waterhouse, A. F., and Coauthors, 2014: Global patterns of diapycnal mixing from measurements
339 of the turbulent dissipation rate. *J. Phys. Oceanogr.*, **44** (7), 1854–1872.
- 340 Waterman, S., A. C. N. Garabato, and K. L. Polzin, 2013: Internal waves and turbulence in the
341 antarctic circumpolar current. *Journal of Physical Oceanography*, **43** (2), 259–282.
- 342 Whalen, C. B., J. A. MacKinnon, L. D. Talley, and A. F. Waterhouse, 2015: Estimating the
343 mean diapycnal mixing using a finescale strain parameterization. *Journal of Physical Oceanog-
344 raphy*, **45** (4), 1174–1188, doi:10.1175/JPO-D-14-0167.1, URL [http://dx.doi.org/10.1175/
345 JPO-D-14-0167.1](http://dx.doi.org/10.1175/JPO-D-14-0167.1).
- 346 Whalen, C. B., L. D. Talley, and J. A. MacKinnon, 2012: Spatial and temporal variabil-
347 ity of global ocean mixing inferred from argo profiles. *Geophys. Res. Lett.*, **39** (L18612),
348 doi:10.1029/2012GL053196.

349 LIST OF FIGURES

350	Fig. 1. Photo of CTD rosette during EQ14 with χ -pods attached.	21
351	Fig. 2. Ratio of the maximum observed wavenumber $k_{max} = f_{max}/u$ to the Batchelor wavenumber 352 k_b for different values of ϵ , assuming a $f_{max} = 7\text{Hz}$. Each line is for a different flowspeed.	22
353	Fig. 3. Portion of a CTD cast showing depth vs time (top) for a portion of an upcast, with data 354 flagged as loops in red. Lower panel shows corresponding χ pod timeseries of dT/dt for 355 that time with discarded loop data in red. Note that variance tends to be larger during depth 356 loops due to entrained water and CTD-induced turbulence.	23
357	Fig. 4. Example timeseries from one CTD cast during EQ14. a) CTD pressure. b) Fallspeed of 358 CTD (dp/dt) .c) Vertical and horizontal accelerations measured by χ -pod. d) Temperature 359 from CTD and (calibrated) χ -pod sensors. T2 is offset slightly for visualization. e) Temper- 360 ature derivative dT/dt measured by the upward-looking χ -pod sensor T1. f) Temperature 361 derivative dT/dt measured by the downward-looking χ -pod sensor T2.	24
362	Fig. 5. Example temperature gradient spectra from EQ14, for high (top) and low (bottom) ϵ . Solid 363 black line with circles show the observed spectra. Dashed line shows the fitted theoretical 364 Kraichnan spectra for the χ pod estimates. Magenta line is Kraichnan spectra for Chameleon 365 χ and ϵ measured at the same depth. Vertical dashed blue(red) lines indicate the minimum 366 (maximum) wavenumber used in the χ pod calculation. The Batchelor wavenumber k_b is 367 also indicated by the vertical cyan line.	25
368	Fig. 6. Depth-time plots of $\log_{10}\chi$ from both methods for EQ14 data. Top: χ pod method. Black 369 diamonds indicate casts used for comparison with CTD- χ pod profiles. Bottom: Chameleon.	26
370	Fig. 7. Left: 2D histogram of $\log_{10}(\chi)$ from Chameleon (x-axis) and χ pod method (y-axes). Values 371 from each profile were averaged in the same 5m depth bins. Right: Normalized histogram 372 of $\log_{10}[\chi_\chi/\chi_\epsilon]$. Vertical dashed line indicates the mean of the the distribution.	27
373	Fig. 8. Left: Scatter plot of χ from CTD- χ pod profiles versus the mean of bracketing Chameleon 374 profiles. Black dashed line shows 1:1, red are $\pm 10\chi$. Right: Normalized histogram of the 375 log of ratios.	28
376	Fig. 9. Histogram of \log_{10} of the ratio of χ for nearby casts. The first set is for the before 377 (cham1) and after (cham2) Chameleon profiles. the 2nd is CTD- χ pod profiles versus the 378 before(cham1) profiles. The last is CTD- χ pod profiles versus the after(cham2) profiles. 379 Dashed lines show the medians of each set. Note that bias is small/zero, and the variability 380 (spread) between CTD/cham is similar to the natural variability between cham profiles.	29
381	Fig. 10. Time mean of χ for all CTD- χ pod - Chameleon cast pairs, with 95% bootstrap confidence 382 intervals.	30
383	Fig. 11. Histogram of % error for χ computed with constant added to fallspeed, in order to examine 384 sensitivity to fallspeed.	31
385	Fig. 12. Left: 2D histograms of χ computed using the interative χ -pod method (top) and the MLE fit 386 (bottom) versus χ computed from Chameleon. Note that the MLE method underestimates 387 χ at larger magnitudes. Right: Histograms of the log of ratios for different ranges of ϵ	32

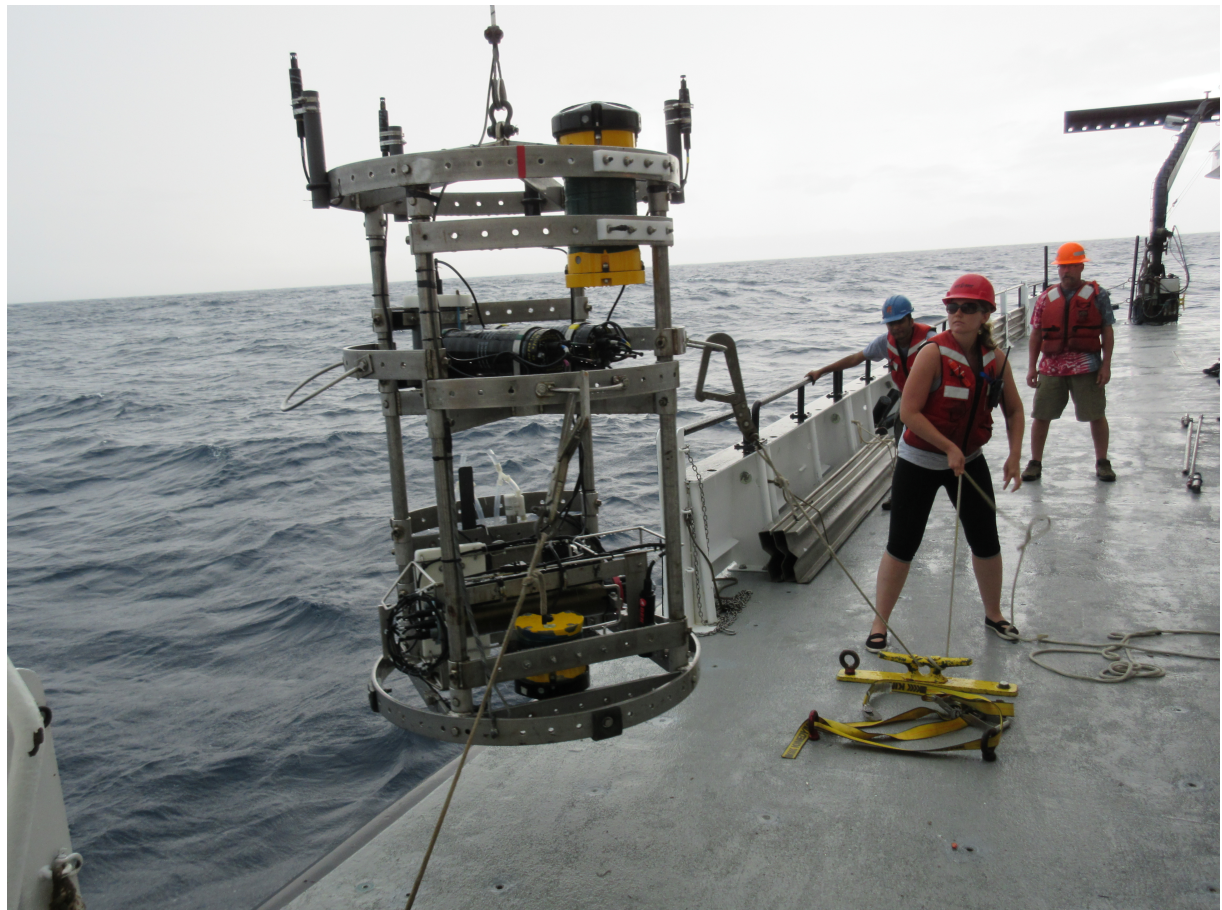
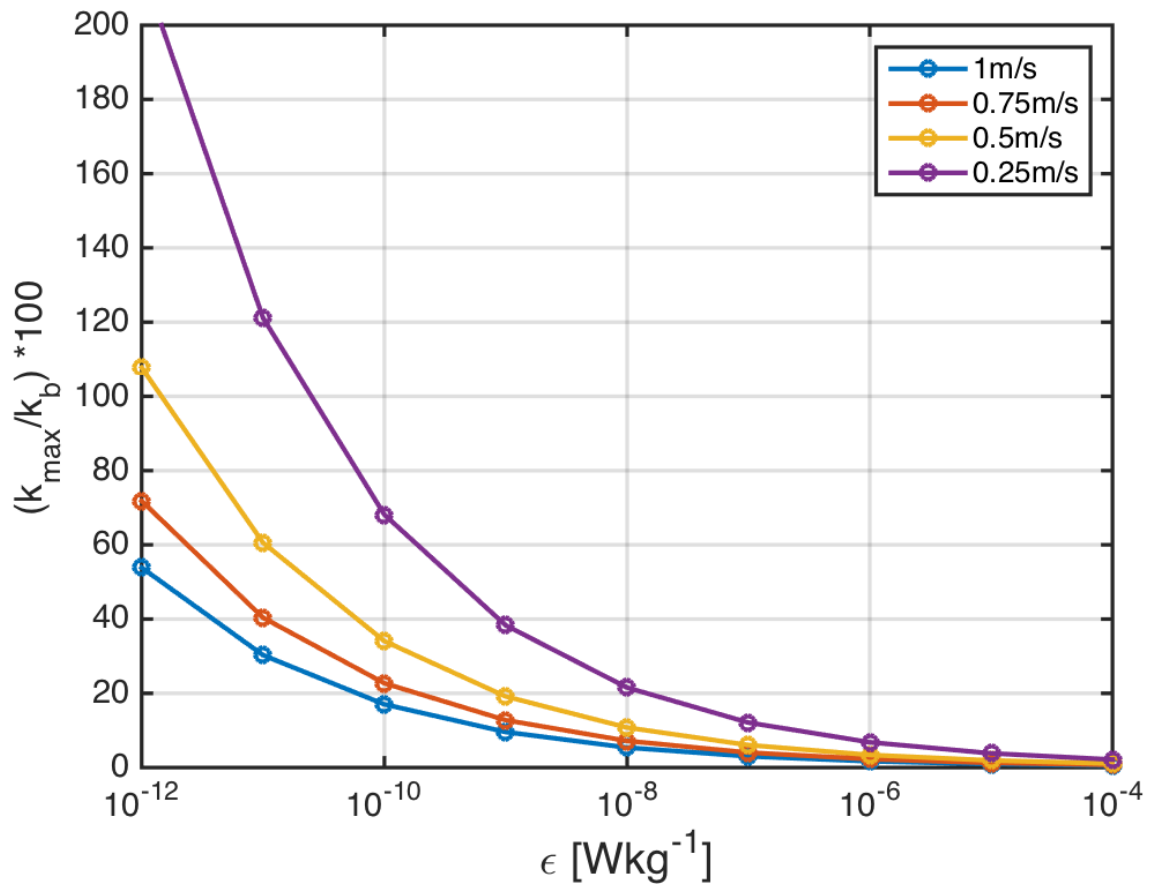
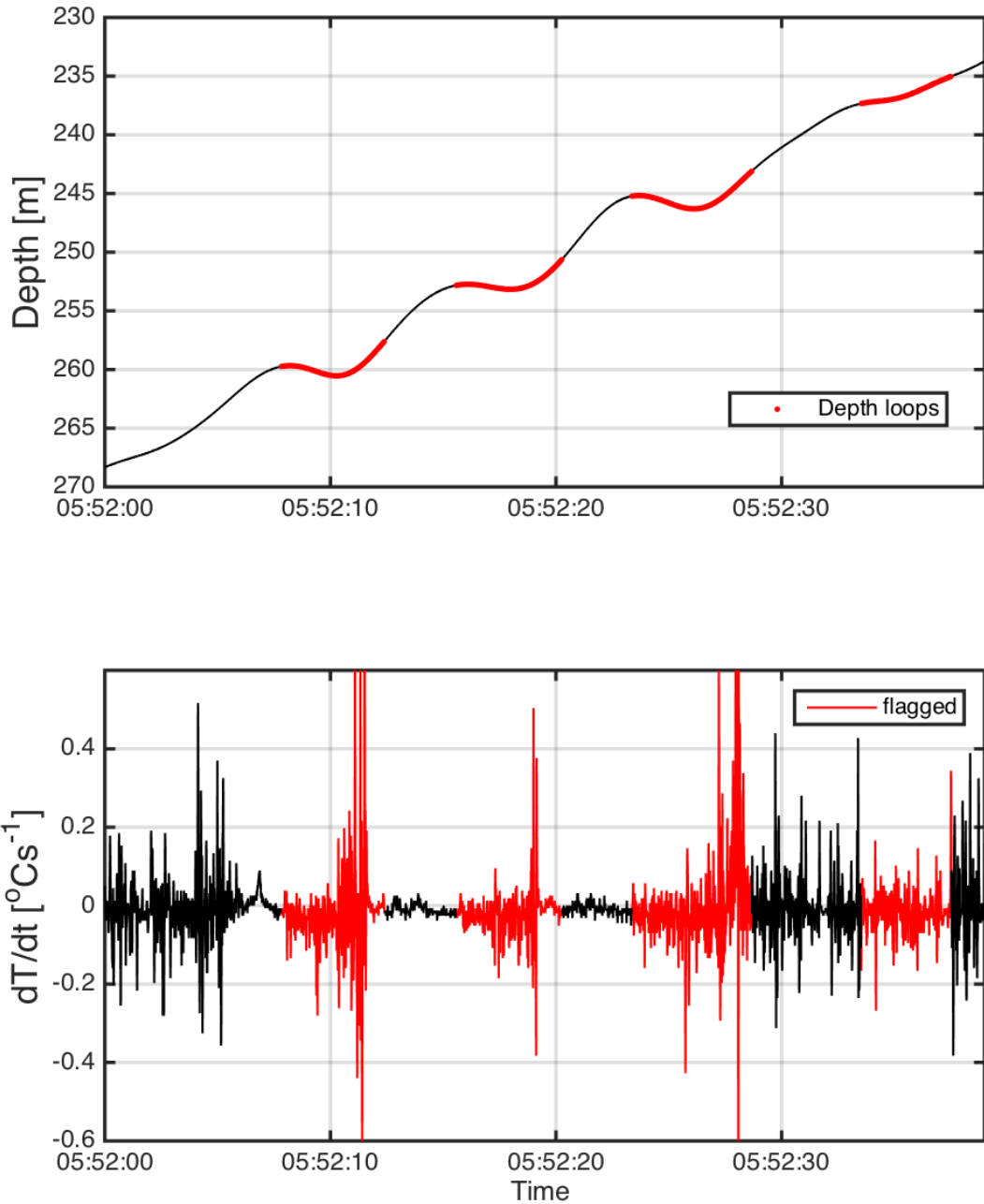


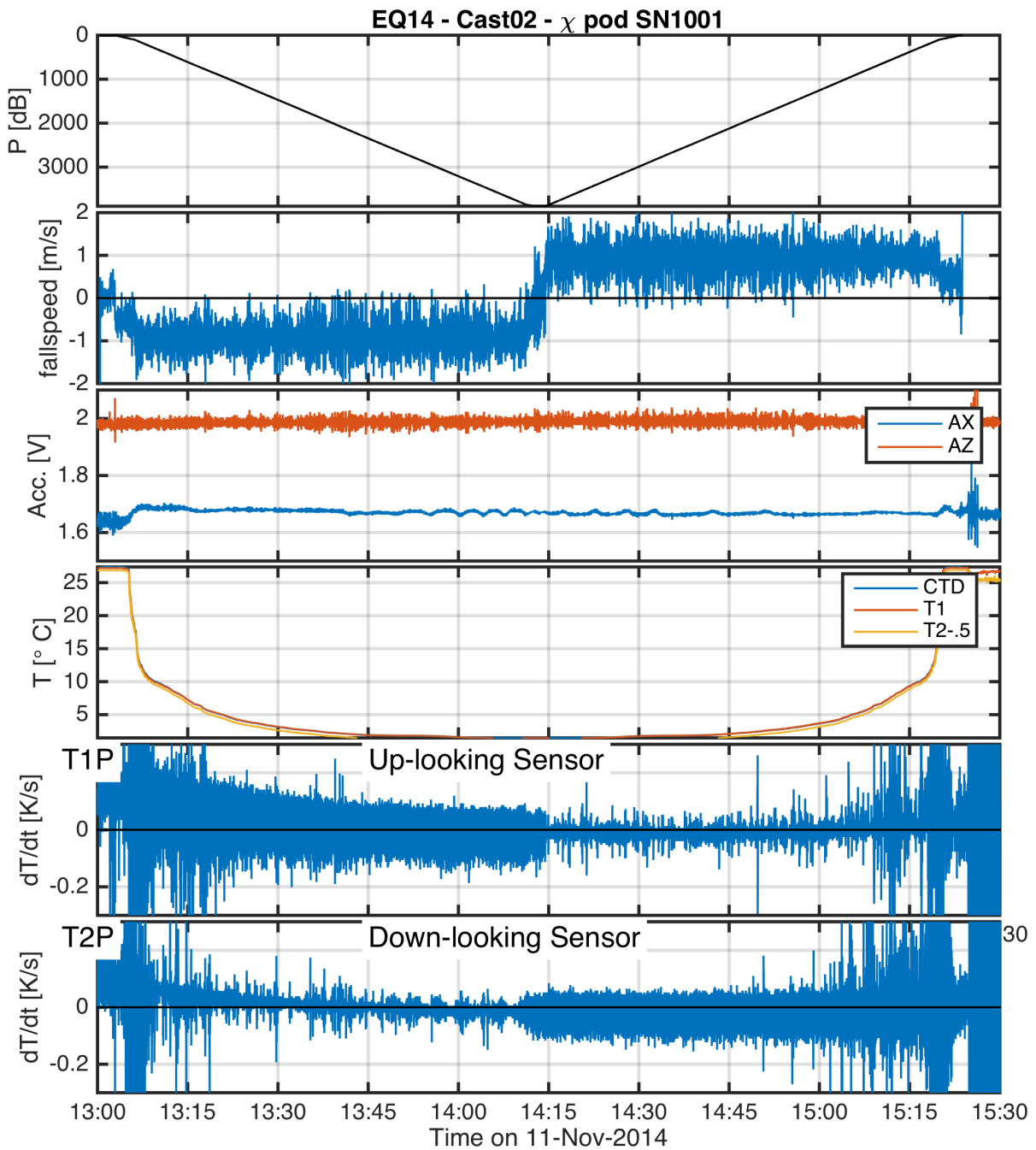
FIG. 1. Photo of CTD rosette during EQ14 with χ -pods attached.



392 FIG. 2. Ratio of the maximum observed wavenumber $k_{\max} = f_{\max}/u$ to the Bachelor wavenumber k_b for
 393 different values of ϵ , assuming a $f_{\max} = 7\text{Hz}$. Each line is for a different flowspeed.



394 FIG. 3. Portion of a CTD cast showing depth vs time (top) for a portion of an upcast, with data flagged as
 395 loops in red. Lower panel shows corresponding χ_{pod} timeseries of dT/dt for that time with discarded loop
 396 data in red. Note that variance tends to be larger during depth loops due to entrained water and CTD-induced
 397 turbulence.



398 FIG. 4. Example timeseries from one CTD cast during EQ14. a) CTD pressure. b) Fallspeed of dp/dt
 399 .c) Vertical and horizontal accelerations measured by χ -pod. d) Temperature from CTD and (calibrated) χ -pod
 400 sensors. T2 is offset slightly for visualization. e) Temperature derivative dT/dt measured by the upward-looking
 401 χ -pod sensor T1. f) Temperature derivative dT/dt measured by the downward-looking χ -pod sensor T2.

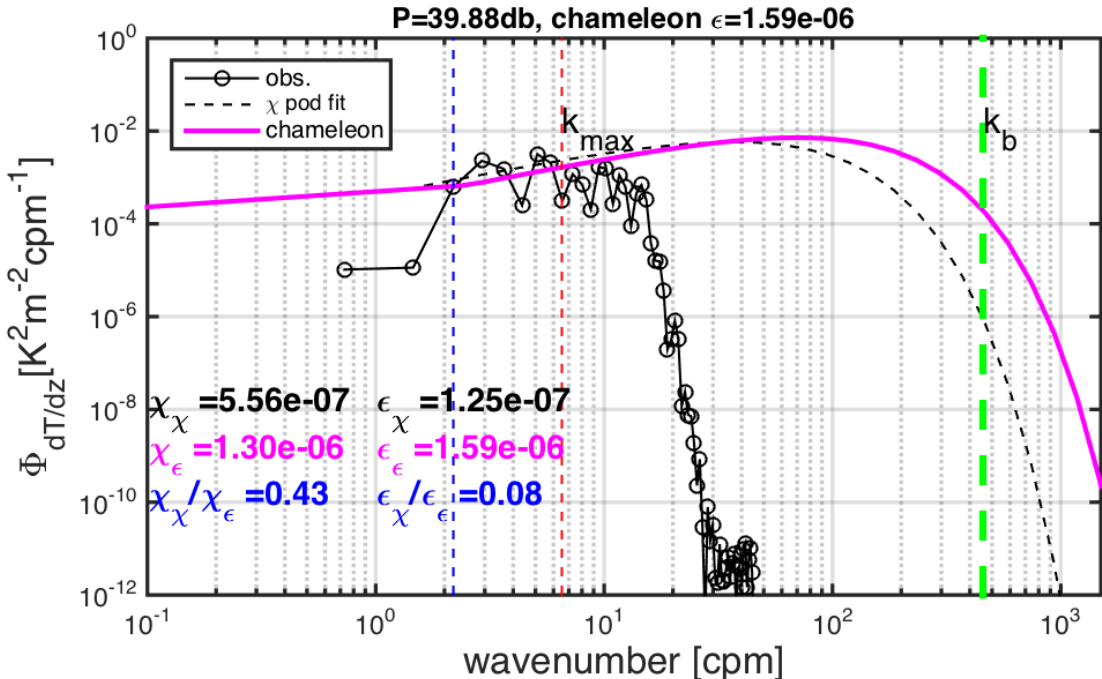
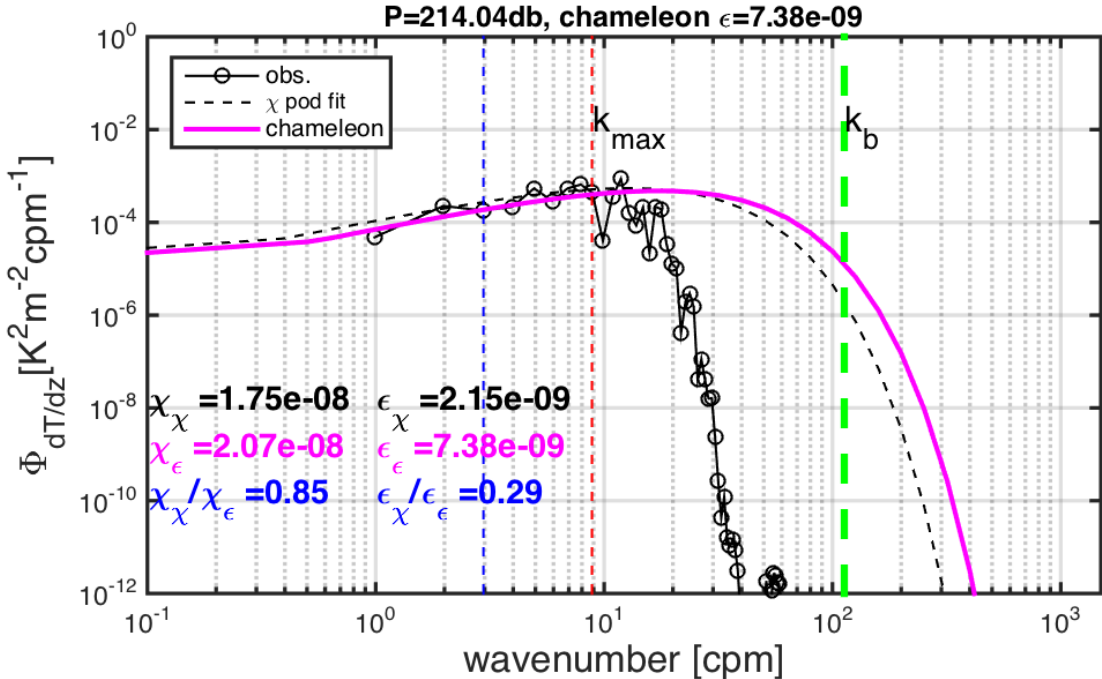
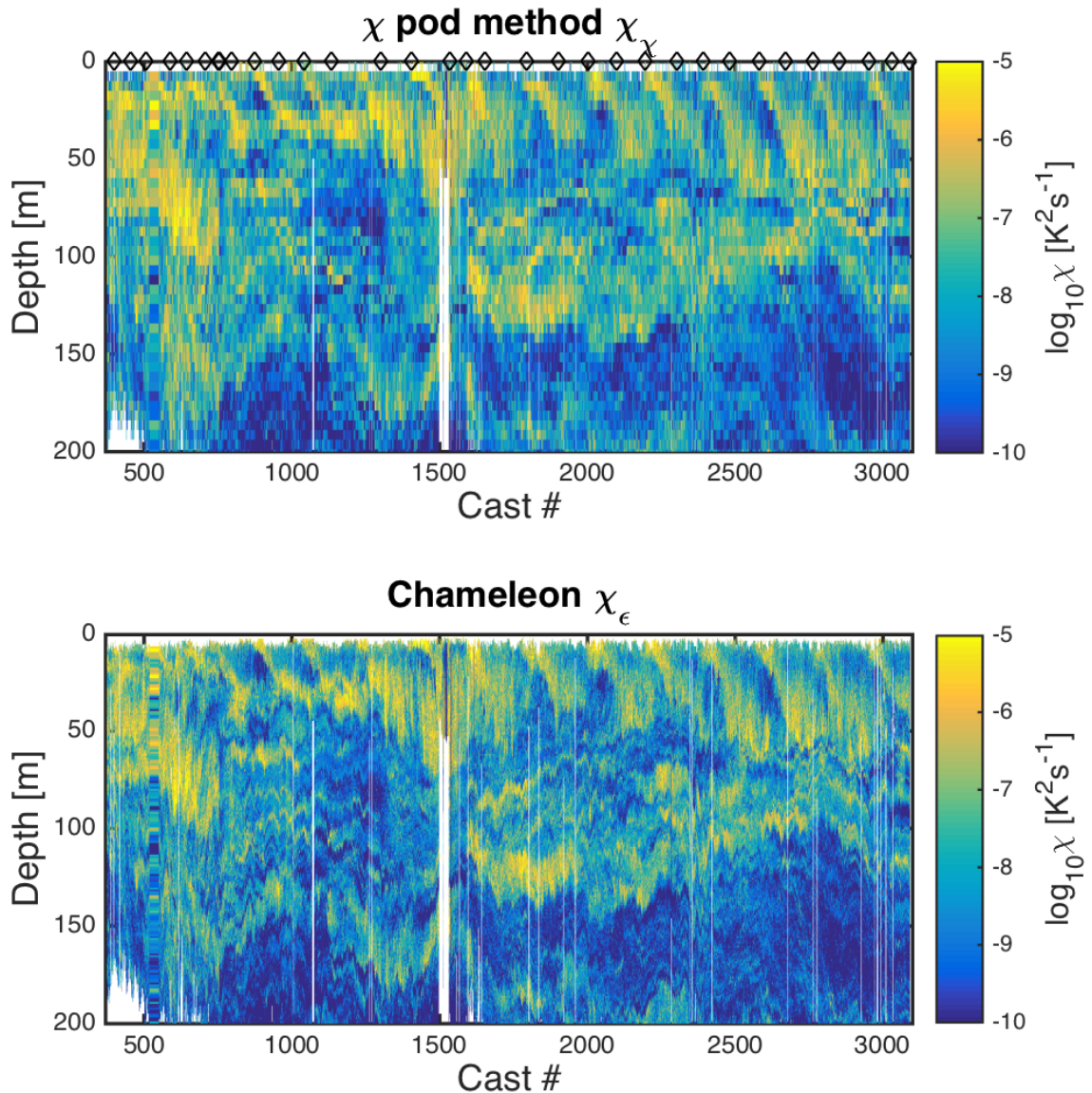
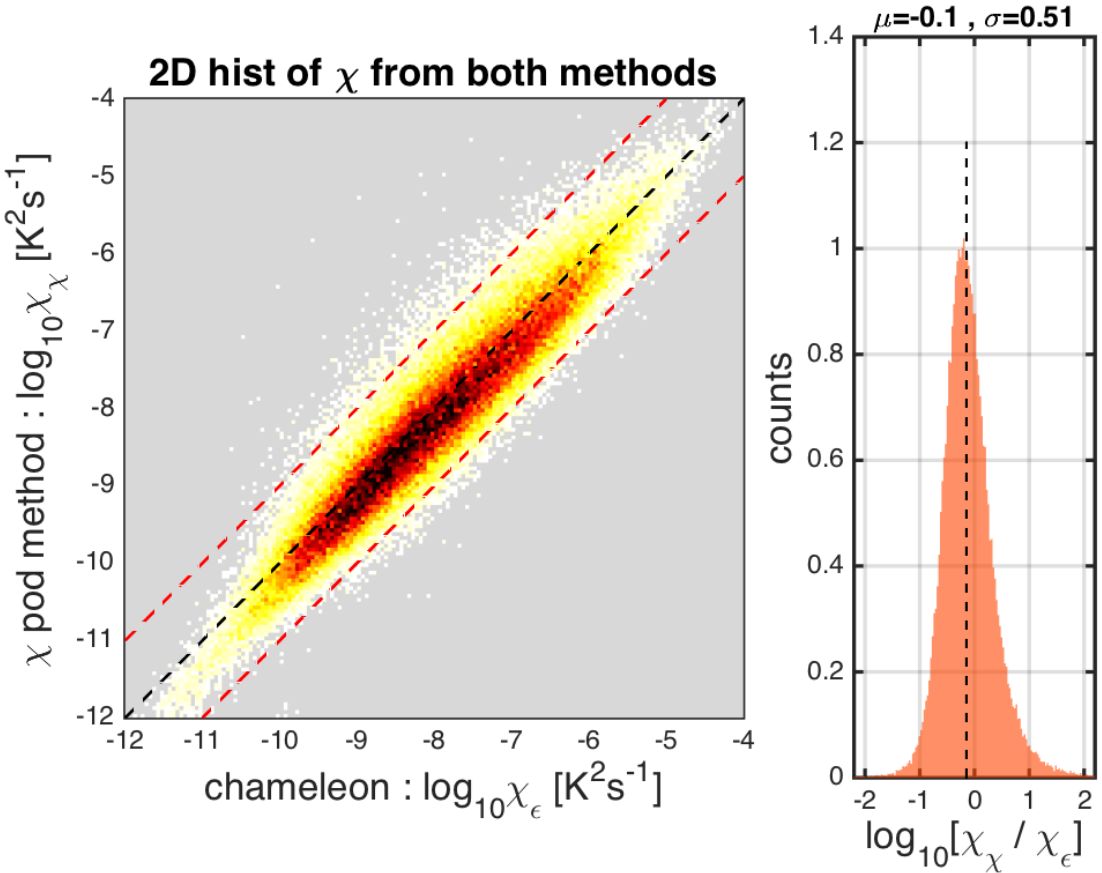


FIG. 5. Example temperature gradient spectra from EQ14, for high (top) and low (bottom) ϵ . Solid black line with circles show the observed spectra. Dashed line shows the fitted theoretical Kraichnan spectra for the χ pod estimates. Magenta line is Kraichnan spectra for Chameleon χ and ϵ measured at the same depth. Vertical dashed blue(red) lines indicate the minimum (maximum) wavenumber used in the χ pod calculation. The Batchelor wavenumber k_b is also indicated by the vertical cyan line.



407 FIG. 6. Depth-time plots of $\log_{10}\chi$ from both methods for EQ14 data. Top: χ_{pod} method. Black diamonds
 408 indicate casts used for comparison with CTD- χ_{pod} profiles. Bottom: Chameleon.



409 FIG. 7. Left: 2D histogram of $\log_{10}(\chi)$ from Chameleon (x-axis) and χ pod method (y-axes). Values from
 410 each profile were averaged in the same 5m depth bins. Right: Normalized histogram of $\log_{10}[\chi_\chi / \chi_\epsilon]$. Vertical
 411 dashed line indicates the mean of the distribution.

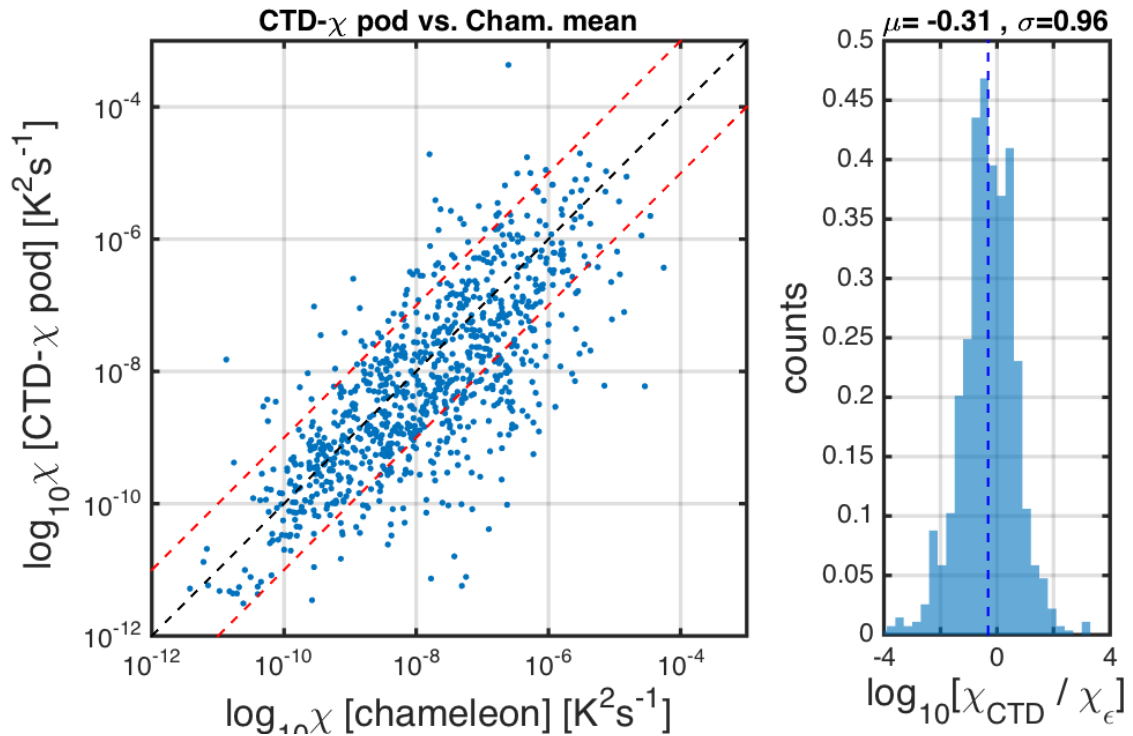


FIG. 8. Left: Scatter plot of χ from CTD- χ pod profiles versus the mean of bracketing Chameleon profiles.
 412 Black dashed line shows 1:1, red are $\pm 10 X$. Right: Normalized histogram of the log of ratios.
 413

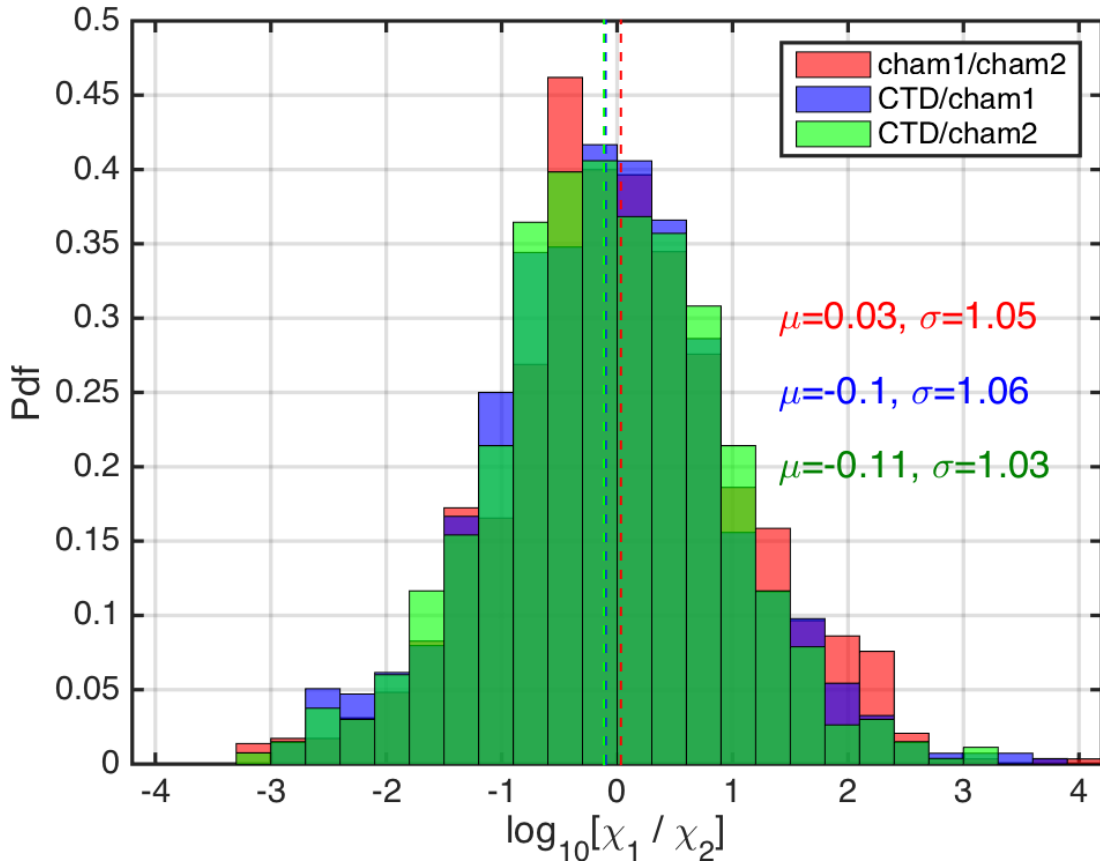


FIG. 9. Histogram of \log_{10} of the ratio of χ for nearby casts. The first set is for the before (cham1) and after (cham2) Chameleon profiles. the 2nd is CTD- χ pod profiles versus the before(cham1) profiles. The last is CTD- χ pod profiles versus the after(cham2) profiles. Dashed lines show the medians of each set. Note that bias is small/zero, and the variability (spread) between CTD/cham is similar to the natural variability between cham profiles.

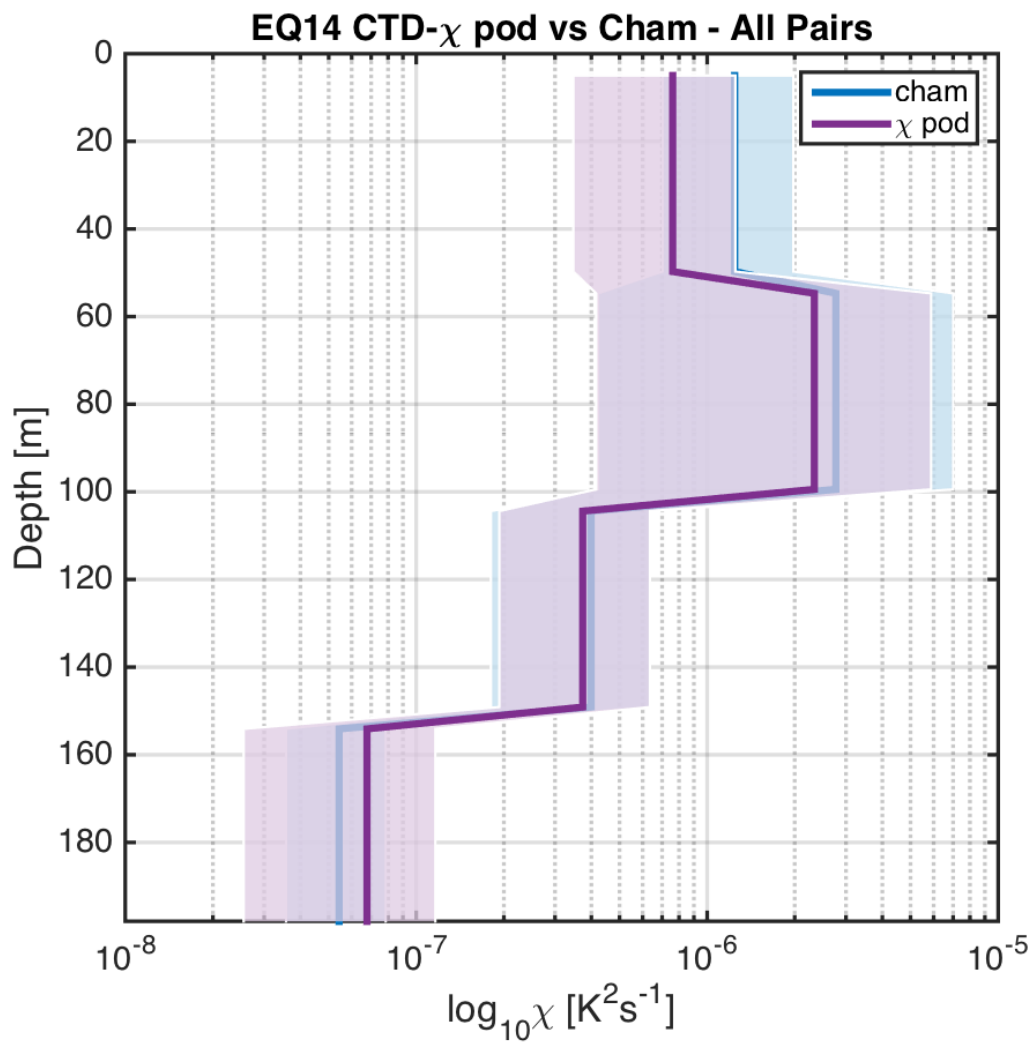
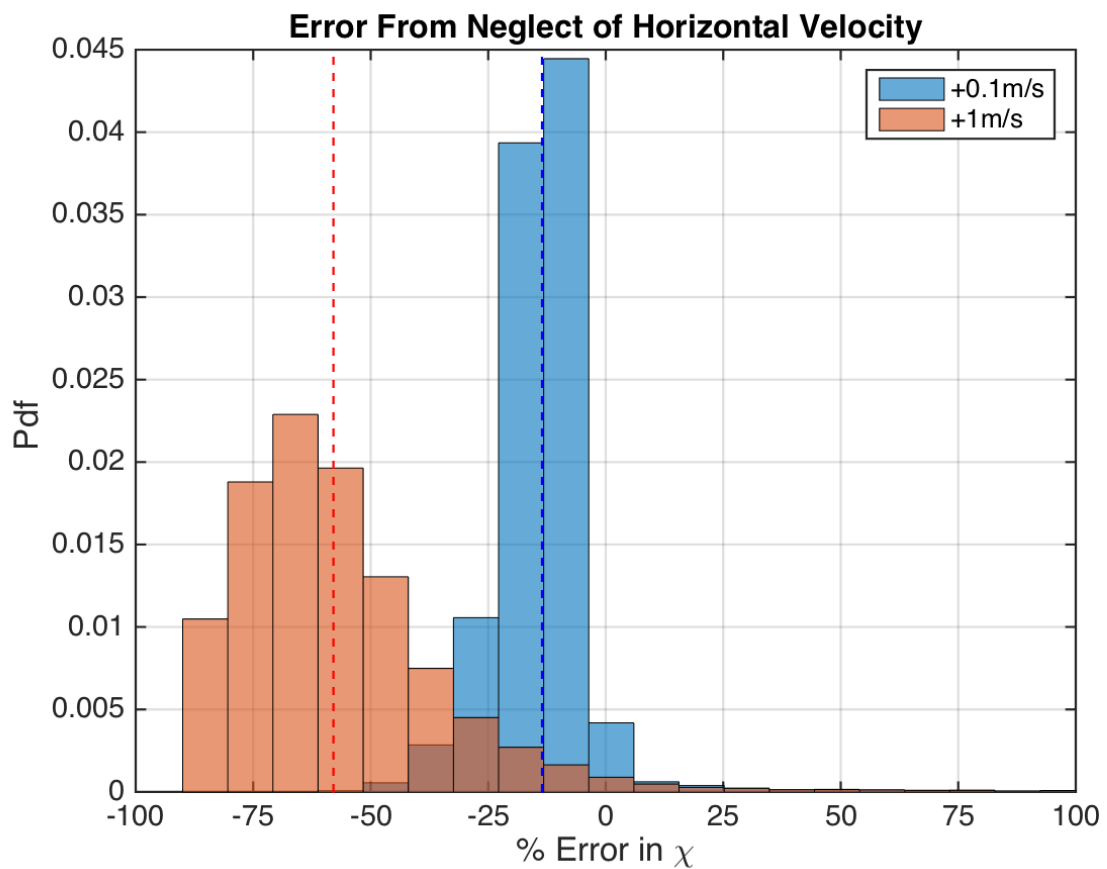
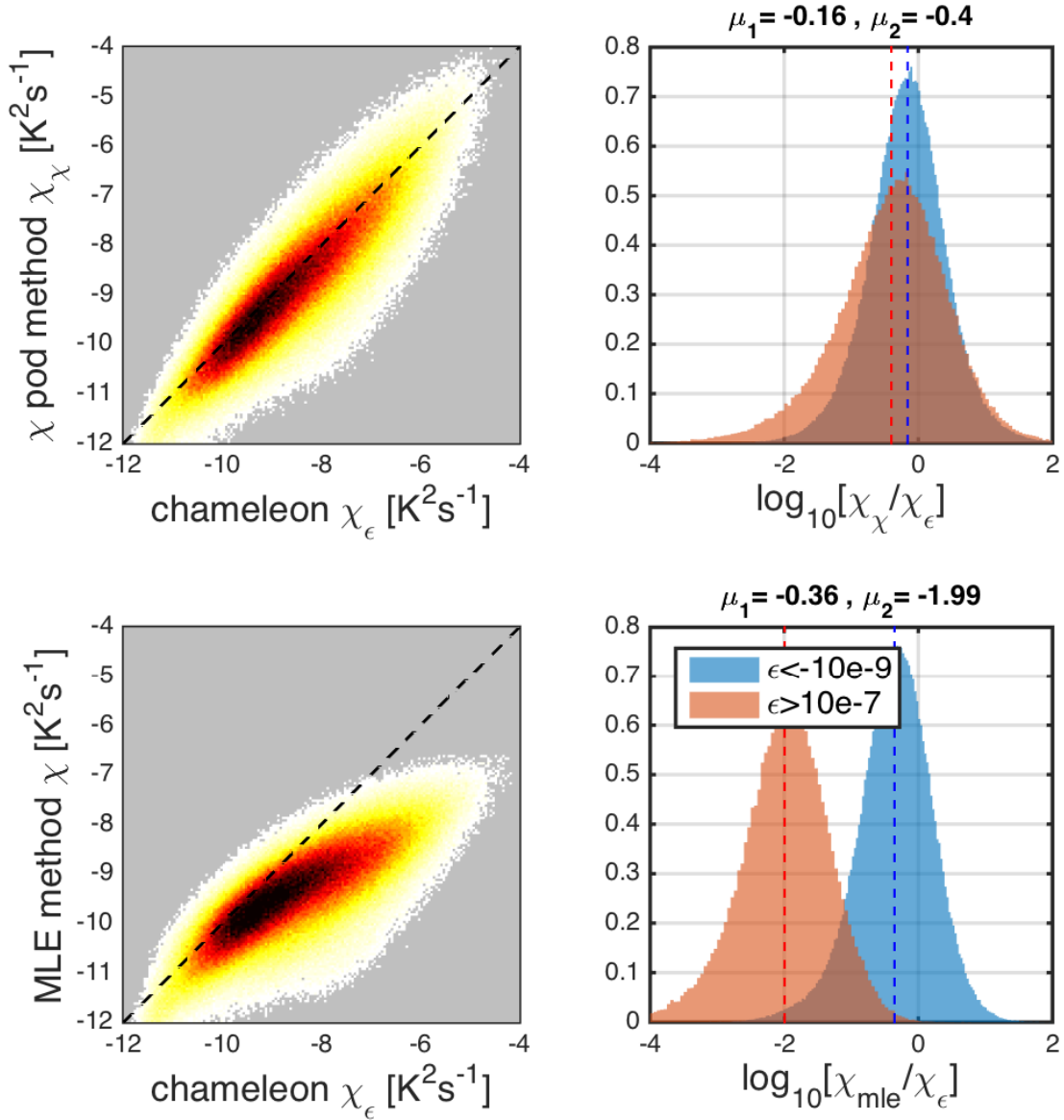


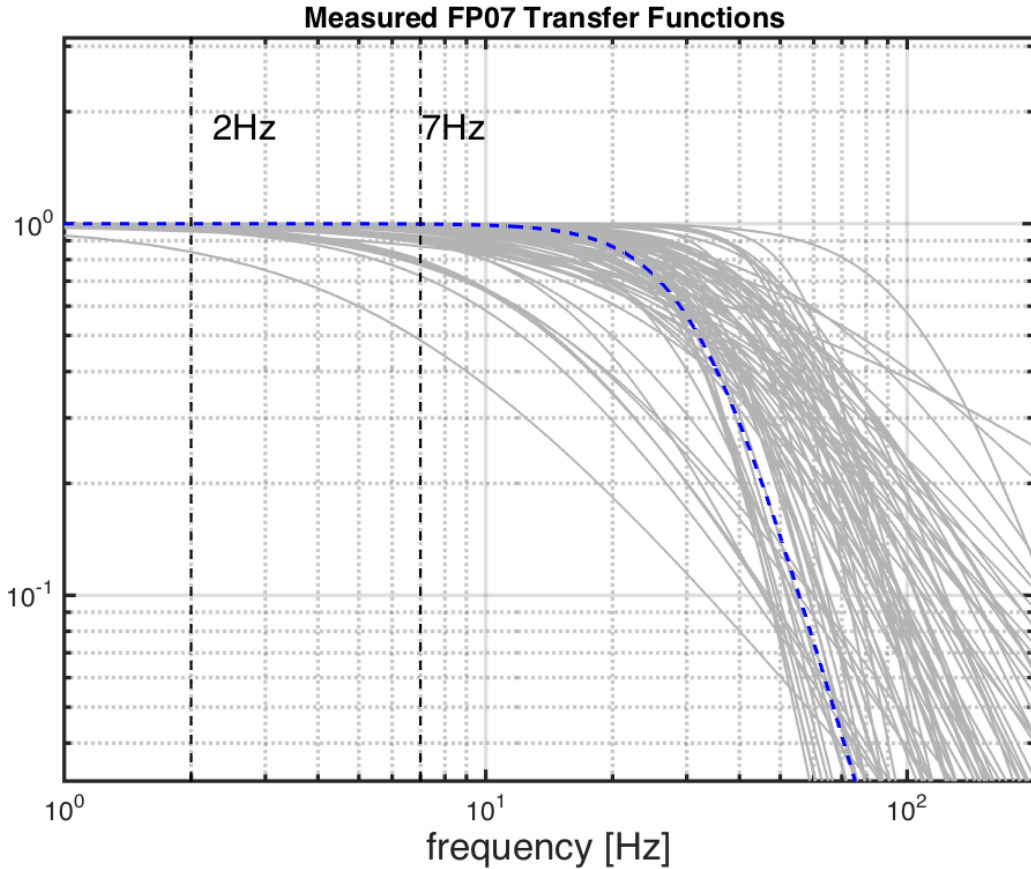
FIG. 10. Time mean of χ for all CTD- χ pod - Chameleon cast pairs, with 95% bootstrap confidence intervals.



419 FIG. 11. Histogram of % error for χ computed with constant added to fallspeed, in order to examine sensitivity
 420 to fallspeed.



421 FIG. 12. Left: 2D histograms of χ computed using the interative χ -pod method (top)
 422 and the MLE fit (bottom) versus χ computed from Chameleon. Note that the MLE method underestimates χ at larger magnitudes. Right:
 423 Histograms of the log of ratios for different ranges of ϵ .



424 FIG. 13. Measured FP07 thermistor transfer functions from historical database. Vertical dashed lines show
 425 the frequency range used in χ pod method. Dashed blue line is a generic transfer function found to best match
 426 measured functions, and is used when response functions are no longer measured.